Poncz, M., Eisman, R., Heidenreich, R., Silver, S. M., Vilaire, G., Surrey, S., Schwartz, E., & Bennett, J. S. (1987) *J. Biol. Chem. 262*, 8476–8482.
Pytela, R., Pierschbacher, M. D., & Ruoslahti, E. (1985a) *Cell (Cambridge, Mass.) 40*, 191–198.
Pytela, R., Pierschbacher, M. D., & Ruoslahti, E. (1985b) *Proc. Natl. Acad. Sci. U.S.A. 82*, 5766–5770.
Pytela, R., Pierschbacher, M. D., Ginsberg, M. H., Plow, E. F., & Ruoslahti, E. (1986) *Science (Washington, D.C.) 231*, 1559–1562.
Ruoslahti, E., & Pierschbacher, M. D. (1986) *Cell (Cambridge, Mass.) 44*, 517–518.
Sanger, F., Nicklen, S., & Coulson, A. R. (1977) *Proc. Natl. Acad. Sci. U.S.A. 74*, 5463–5466.
Springer, T. A., & Anderson, D. C. (1985) in *Hybridoma Technology in the Biosciences and Medicine* (Springer, T. A., Ed.) pp 191–206, Plenum Press, New York.
Stephens, R. E. (1975) *Anal. Biochem. 65*, 369–379.
Suzuki, S., Argraves, W. S., Pytela, R., Arai, H., Krusius, T., Pierschbacher, M. D., & Ruoslahti, E. (1986) *Proc. Natl. Acad. Sci. U.S.A. 83*, 8614–8618.
Takada, Y., Huang, C., & Hemler, M. E. (1987a) *Nature (London) 326*, 607–609.
Takada, Y., Strominger, J. L., & Hemler, M. E. (1987b) *Proc. Natl. Acad. Sci. U.S.A. 84*, 3239–3243.
Tamkun, J. W., DeSimone, D. W., Fonda, D., Patel, R. S., Buck, C., Horwitz, A. F., & Hynes, R. O. (1986) *Cell (Cambridge, Mass.) 46*, 271–282.
Thiagarajan, P., Shapiro, S. S., Levine, E., DeMarco, L., & Yalcin, A. (1985) *J. Clin. Invest. 75*, 896–901.
Weisgraber, K. H., Rall, S. C., Jr., & Mahley, R. W. (1981) *J. Biol. Chem. 256*, 9077–9083.
Wilcox, M., & Leptin, M. (1985) *Nature (London) 316*, 351–354.
Wright, S. D., Reddy, P. A., Jong, M. T. C., & Erickson, B. W. (1987) *Proc. Natl. Acad. Sci. U.S.A. 84*, 1965–1968.
Young, R. A., & Davis, R. W. (1983) *Proc. Natl. Acad. Sci. U.S.A. 80*, 1194–1198.

Crystal Structures of Metyrapone- and Phenylimidazole-Inhibited Complexes of Cytochrome P-450$_{cam}$†

Thomas L. Poulos* and Andrew J. Howard
Protein Engineering Department, Genex Corporation, Gaithersburg, Maryland 20877
Received February 18, 1987; Revised Manuscript Received June 15, 1987

ABSTRACT: The crystal structures of metyrapone- and 1-, 2-, and 4-phenylimidazole-inhibited complexes of cytochrome P-450$_{cam}$ have been refined to a nominal resolution of 2.1 Å and compared with the 1.63-Å camphor-bound structure. With the exception of 2-phenylimidazole, each of the inhibitors forms an N–Fe bond with the heme iron atom while part of the inhibitor sits in the camphor-binding pocket. In the 2-phenylimidazole complex, a water molecule or hydroxide ion coordinates with the heme iron atom while the inhibitor binds in the camphor pocket adjacent to the aqua ligand. Each of the inhibitors forces the central region of helix I that forms part of the O_2 binding pocket to move away from the inhibitor, with the exception of 2-phenylimidazole where the helix moves in toward the inhibitor. In addition, the Tyr-96 region, which provides specific contact points with the substrate, is perturbed, although to varying degrees with each inhibitor. These perturbations include large, localized changes in Debye–Waller or temperature factors, indicative of changes in dynamical fluctuations. The largest inhibitor, metyrapone, causes the fewest changes, while 2-phenylimidazole binding causes the largest, especially in helix I. The large 2-phenylimidazole-induced movement of helix I can be rationalized on the basis of the inhibitor imidazole group's hydrogen-bonding requirements.

Cytochromes P-450 are a widely occurring class of *b*-type heme proteins that catalyze the hydroxylation of both aliphatic and aromatic molecules (Hayaishi, 1974). Much of what is known about the details of cytochrome P-450 structure and function stems from studies with cytochrome P-450$_{cam}$ obtained from the soil bacteria *Pseudomonas putida* (Wagner & Gunsalus, 1982; Gunsalus et al., 1974; Debrunner et al., 1978; Gunsalus & Sligar, 1978). P-450$_{cam}$ catalyzes the conversion of camphor to 5-*exo*-hydroxycamphor (Gelb et al., 1982) and is the first step in the oxidative assimilation of camphor when camphor is utilized by *P. putida* as a carbon source (Gunsalus et al., 1974).

The crystal structure of P-450$_{cam}$ has been determined with substrate bound first at 2.6 Å (Poulos et al., 1985) and then 1.63 Å (Poulos et al., 1987). In addition, the substrate-free structure has been refined at 2.1 Å (Poulos et al., 1986). The substrate, camphor, contacts the heme ring immediately adjacent to the oxygen-binding site and is held in place by complementary contacts with neighboring aliphatic and aromatic residues in addition to a single hydrogen bond between the camphor carbonyl oxygen atom and the hydroxyl group of Tyr-96. When camphor is bound, the high-spin heme iron atom is pentacoordinate with the sulfur atom of Cys-357 serving as the only axial ligand (Poulos et al., 1985). In the absence of camphor, the substrate pocket fills with a hydrogen-bonded array of solvent molecules, one of which coordinates with the iron atom (Poulos et al., 1986), giving a hexacoordinate, low-spin heme. No significant conformational

† This work was supported in part by NIH Grant GM 33688.
* Address correspondence to this author at the Center for Advanced Research in Biotechnology, 9600 Gudelsky Drive, Rockville, MD 20850.

0006-2960/87/0426-8165$01.50/0

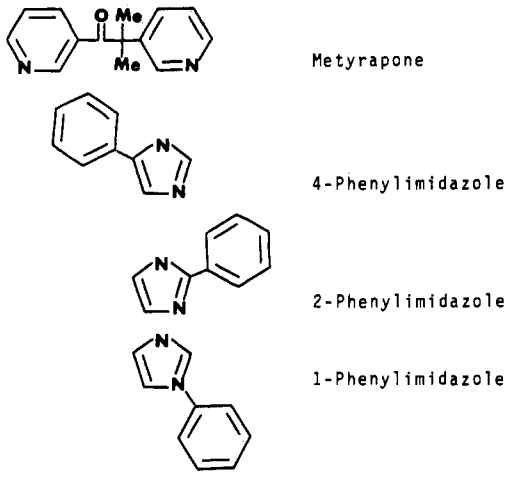

FIGURE 1: Structures of the inhibitors used in this study.

change accompanies the conversion of substrate-free to substrate-bound P-450$_{cam}$. However, an analysis of changes in the temperature factors revealed that segments of P-450$_{cam}$ contacting the substrate undergo large increases in thermal motion in the substrate-free form of the enzyme. Moreover, these regions define a small opening at the molecular surface that very likely serves as a substrate access channel. It therefore appears that enhanced dynamical fluctuations of the access route allow for the entry of a substrate molecule into the active site.

These results indicate a certain degree of flexibility in and near the substrate-binding pocket. Ideally, we would like to trap the access channel in the open configuration in order to determine more precisely the range of motions possible. We reasoned that molecules larger than or shaped differently from camphor and which are known to bind at the camphor site might enter via the same route as camphor and cause distortions at or near the substrate pocket. Such changes could enable us to gain some further insight into the mechanics and dynamics of substrate binding. In searching for molecules that would induce the desired perturbations, we turned to those containing aromatic nitrogen atoms like pyridines and imidazoles. Such molecules form low-spin complexes with P-450$_{cam}$ owing to direct coordination of a heterocyclic nitrogen atom with the iron atom (Lipscomb, 1980; Dawson et al., 1982). The complexes formed with metyrapone, a well-known P-450 inhibitor (Testa & Jenner, 1981; Dominguez & Samuels, 1963), and phenylimidazoles have been spectrally well characterized (Lipscomb, 1983; Dawson et al., 1982) and are ideally suited as P-450 active-site probes. Here we report the crystal structures of four such complexes.

Materials and Methods

P-450$_{cam}$ was crystallized in the absence of camphor according to our earlier procedure (Poulos et al., 1982). The inhibitors used in this study were metyrapone and the 1-, 2-, and 4-isomers of phenylimidazole (structures shown in Figure 1). Inhibitor–P-450 complexes were formed by soaking crystals at room temperatures in 40% ammonium sulfate, 0.2 M KCl, 0.050 M potassium phosphate, pH 7.0, and 1 mM inhibitor. The solution was changed every 2 days over a 2-week period.

X-ray intensity data were obtained with a Xentronics area detector and a GX-21 rotating anode X-ray source operating at 2.8 kW. The XENGEN package of software was used for data reduction (Howard, unpublished data). A single crystal was used to obtain each set of data to a maximum resolution of 2.1 Å. For each of the crystals, approximately 85% of the possible data to 2.3 Å were collected, while about 40% of the data in the 2.3–2.1 Å shell were collected. Table I summarizes additional data collection statistics.

Table I: Summary of Data Collection

	total obsd	R_{sym}[a]	unique data	max resolution (Å)	possible data to max resolution
metyrapone	57062	0.057	19243	2.13	24027
1-phenyl-imidazole	60532	0.048	17735	2.09	25652
2-phenyl-imidazole	60967	0.059	19199	2.14	23698
4-phenyl-imidazole	56269	0.051	21899	2.07	25652

[a] $R_{sym} = \sum|I_i - \langle I_i\rangle|/\sum I_i$, where I_i = intensity of ith observation and $\langle I_i\rangle$ = mean intensity.

Crystallographic refinement was carried out by use of the restrained parameters least-squares package of programs (Hendrickson & Konnert, 1980). In each case, the starting model for refinement was the refined (R = 0.19) 1.63-Å camphor-bound structure. Refinement was judged complete when $F_o - F_c$[1] difference maps indicated no further changes to the model. Each of the models was tightly constrained to conform to ideal bond distances and angles. A summary of the crystallographic refinements is given in Table II.

Results

Initial Difference Fouriers

Before describing our results, we briefly review those aspects of the P-450$_{cam}$ structure relevant to this study. A schematic representation of the P-450$_{cam}$ molecule is shown in Figure 2. The camphor molecule sits just above the heme and is hidden from view in Figure 2 by helix F. The axial heme ligand, Cys-357, is situated at the C-terminal end of an antiparallel β pair highlighted as the shaded arrows in Figure 2, and it, too, is hidden from view. The longest helix in the structure, helix I or the distal helix, runs through the center of the molecule and contacts both the heme and camphor. As we will describe in more detail below, the central region of helix I forms part of the O_2 binding pocket.

$F_o - F_c$ difference Fouriers were computed for each complex by carrying out structure factor calculations using data obtained from the inhibitor complexes and coordinates taken from the refined (R = 0.19) 1.63-Å camphor-bound structure but which lacked the camphor coordinates. Removing the camphor atoms from the structure factor calculations gave $F_o - F_c$ maps that were not obscured in regions where camphor and inhibitor atoms overlap. The resulting electron density difference maps are shown in Figure 3. In each case, positive $F_o - F_c$ difference density indicates clearly the presence of the inhibitor, enabling a straightforward fit of inhibitor molecular models to the electron density. The maps in Figure 3 reveal two additional key features. First, a heterocyclic nitrogen atom of the inhibitor coordinates with the iron atom except with 2-phenylimidazole. As Figure 3C illustrates, 2-phenylimidazole binds in the camphor pocket adjacent to the oxygen-binding site, while an isolated lobe of positive density linked to the iron atom indicates a coordinated water molecule or hydroxide ion. Second, positive and negative features surrounding protein groups demonstrate considerable perturbation of surrounding protein atoms. The largest inhibitor,

[1] Abbreviations: F_o, observed structure factor; F_c, calculated structure factor; rms, root mean square.

Table II: Summary of Crystallographic Refinement and Root Mean Square Fit between the Inhibited and Camphor-Bound Structures

derivative	resolution range (Å)	reflections measured	reflections used, $I > \sigma(I)$	R factor[a]	rms deviations of final model[b] (Å)	rms fit between inhibited and camphor-bound structures[c] (Å)	
						main chain	side chain
metyrapone	10–2.13	19243	14954	0.16	0.019	0.133	0.159
1-phenylimidazole	10–2.09	17736	13803	0.17	0.021	0.181	0.251
2-phenylimidazole	10–2.14	19199	14492	0.18	0.021	0.192	0.274
4-phenylimidazole	10–2.07	21899	16207	0.18	0.019	0.208	0.32

[a] R factor = $\sum|F_o - F_c|/\sum F_o$. [b] The rms deviation of the final model represents the root mean square deviation of the final refined model from bond distances expected from small molecule crystal structures. [c] The rms fit between the inhibited and camphor-bound structures is the result of a least-squares superimposition of the two structures and the values in the table refer to the root mean square fit between main-chain and side-chain atoms.

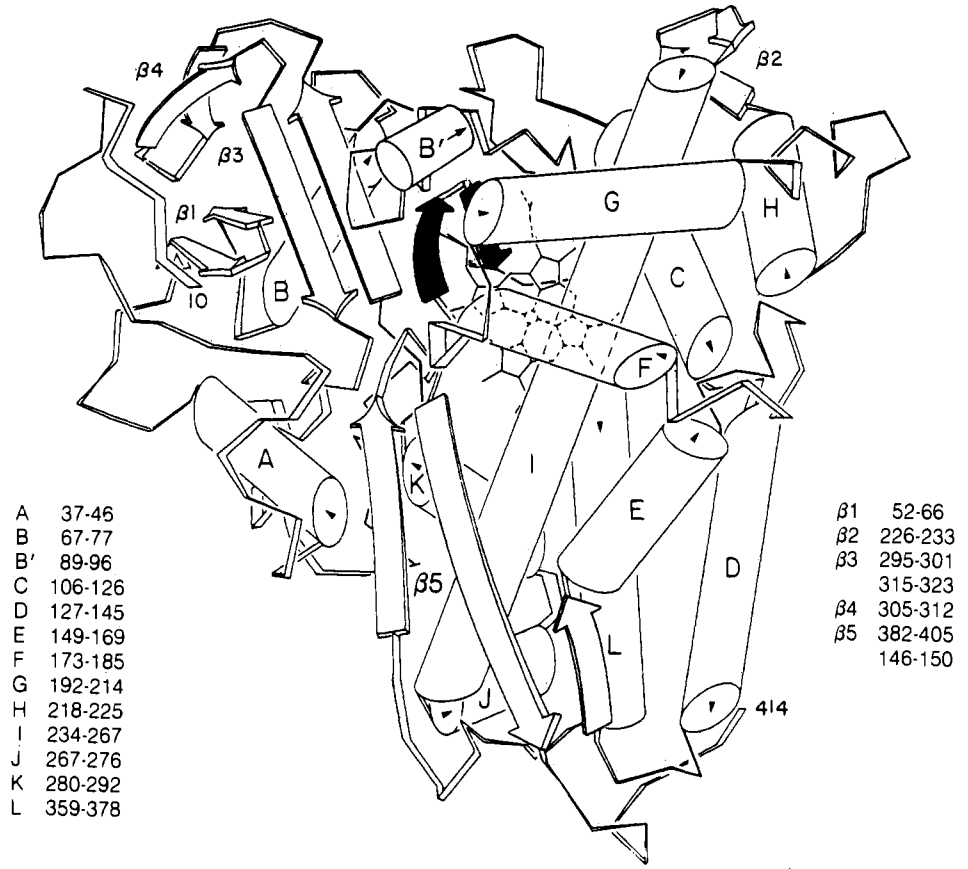

FIGURE 2: Schematic representation of P-450$_{cam}$. Helices are indicated by bars and β structure by ribbons. The shaded region highlights the antiparallel β pair and β bulge that contain the axial heme ligand, Cys-357. Those regions undergoing enhanced thermal fluctuations in the absence of substrate and that define the proposed substrate access channel include the following: the N-terminal end of helix B′; the elongated stretch connecting helices F and G; and the turn connecting the antiparallel strand of β5 centered on residue 395.

metyrapone, leads to the fewest changes, while the nonliganded inhibitor 2-phenylimidazole results in the largest perturbations.

Crystallographic Refinement

To better quantitate conformational changes, each structure was refined until $F_o - F_c$ difference maps indicated no further changes to the model and the R factor had converged. Refinement cycles were interspersed with frequent examination of F_o–F_c and $2F_o$–F_c electron density maps. With 2- and 4-phenylimidazoles it was necessary to manually adjust protein groups during the refinement.

Comparison of the Refined Structures

Methods of Comparisons. Refined atomic coordinates for each structure were compared with the native structure by a least-squares fit procedure giving a root mean square deviation of main-chain and side-chain atoms (Honzatko, 1986). These data are presented in Table II. Shifts in main-chain and side-chain atoms also were plotted as a function of residue number to provide a simple graphical representation of conformational changes (not shown). These plots coupled with visual examination of superimposed molecular models in a graphics system showed that inhibitor-induced movement was confined primarily to the central segment of helix I and the region surrounding Tyr-96. Figure 4 depicts molecular models of the inhibited complexes superimposed on the native structure.

We also compared Debye–Waller or temperature factors. Crystallographic temperature factors can provide useful information about protein dynamics (Karplus & McCammon, 1983; van Gunsteren & Karplus, 1981) but are complex quantities that also contain contributions from crystalline lattice effects in addition to errors in both intensities and models (Finzel & Salemme, 1985; Frauenfelder et al., 1979). As we discussed in our description of the camphor-free structure, temperature factor differences will reflect primarily dynamical fluctuation changes if the data being compared are obtained from isomorphous crystals collected at the same

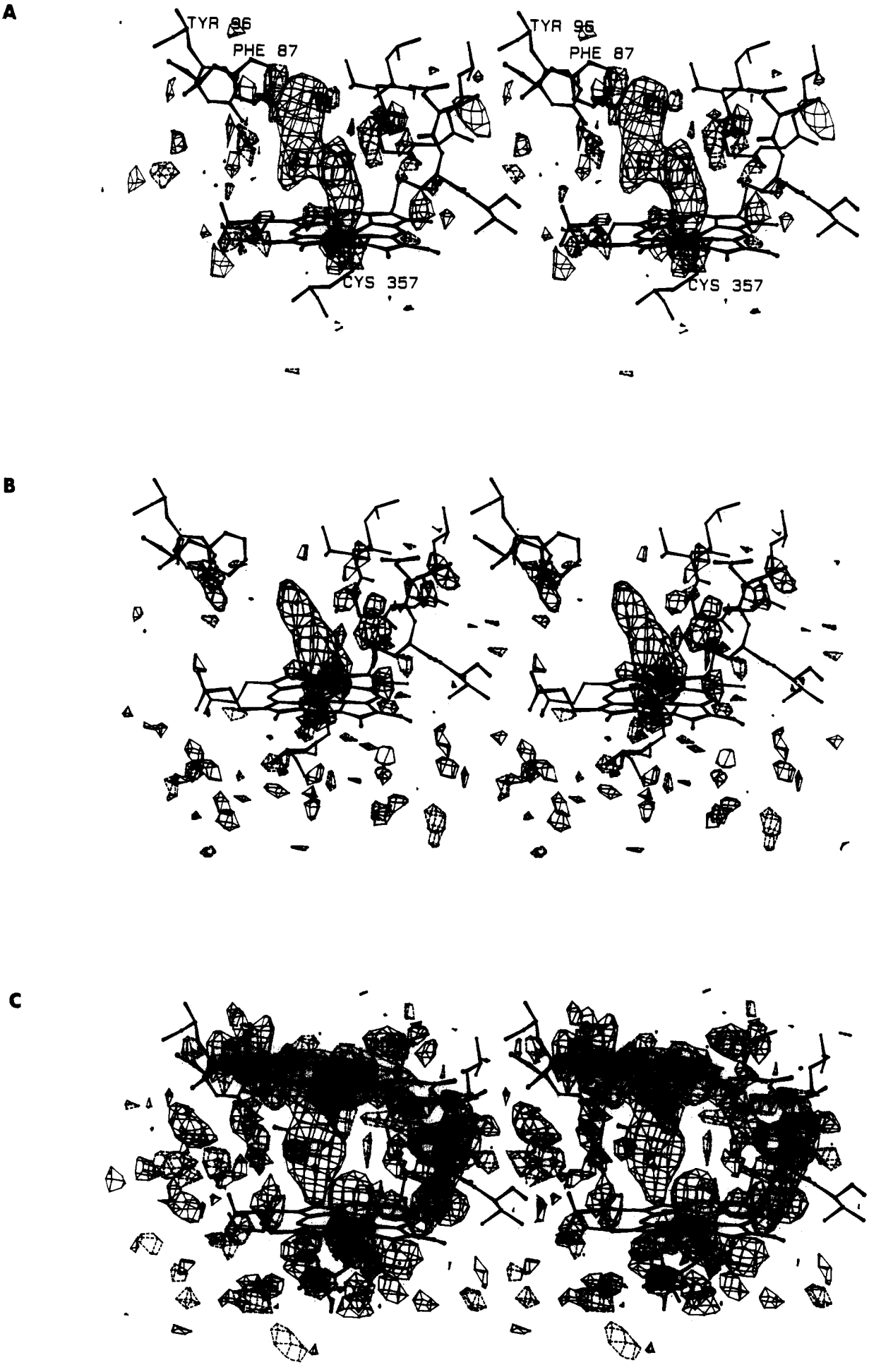
A
TYR 96
PHE 87
CYS 357
TYR 96
PHE 87
CYS 357
B
C

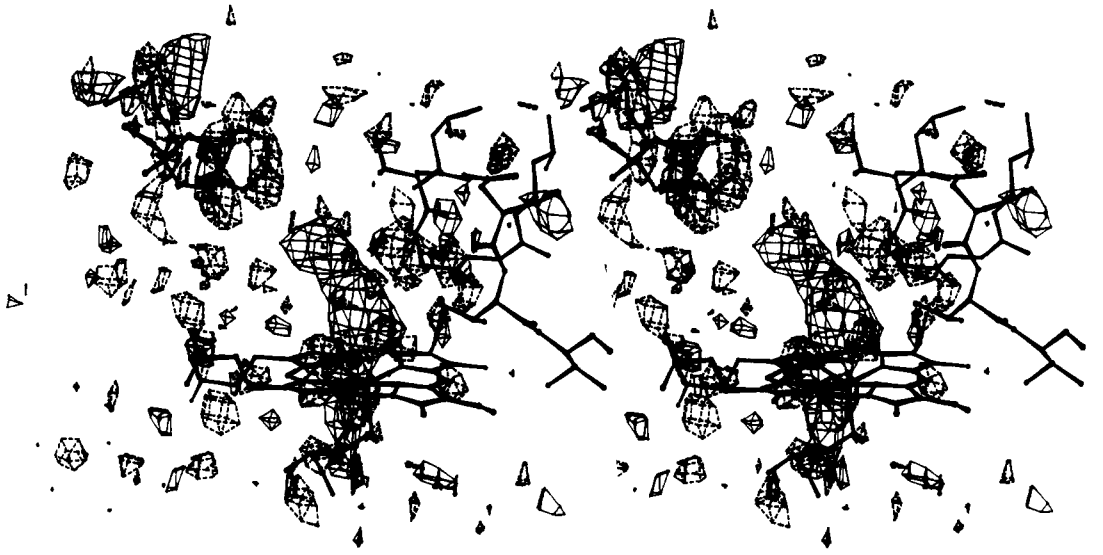

FIGURE 3: Initial $F_o - F_c$ electron density difference maps superimposed on the active-site regions. The maps were contoured at $\pm 3\sigma$ levels, where σ represents the root mean square difference density taken over an entire asymmetric unit. Negative contours are shown as dashed lines and positive contours as solid lines. (A) Metyrapone; (B) 1-phenylimidazole; (C) 2-phenylimidazole; and (D) 4-phenylimidazole.

temperature (Poulos et al., 1986). Thus, the temperature factor plots shown in Figure 5 provide useful information about which regions of the structure undergo alterations in dynamical fluctuations owing to inhibitor binding. In Figure 5, the mean temperature factor for each residue was computed and then the difference in mean temperature factor between the inhibited and native (inhibitor–native) complexes plotted against residue number.

Metyrapone. The structure of metyrapone (Figure 1) suggests that either of the two pyridine-ring nitrogen atoms should be able to coordinate with the iron atom, and we anticipated a mixture of both possibilities. However, the excellent fit of metyrapone to the initial $F_o - F_c$ map and the final $2F_o - F_c$ map demonstrates only one orientation. The reason for the preferred binding mode of metyrapone is probably due to steric constraints. When a model was built with the opposite orientation with N2 liganded to the iron atom, it became evident that the two metyrapone methyl groups would approach both Val-396 and Val-295 (shown in Figure 6B) to within less than 2.8 Å. On the other hand, in the orientation shown in Figure 6B with N1 liganded to the iron atom, the metyrapone carbonyl oxygen atom is situated near Val-295 and Val-396 at distances of 3.3 and 4.0 Å, respectively, while the closest contact with an inhibitor methyl group is with Ile-395, a distance of about 3.5 Å. Another unanticipated structural characteristic of metyrapone binding was the observed interaction between N2 and Tyr-96 (Figure 6). The Tyr-96 side-chain hydroxyl group is in position to donate a hydrogen bond to the metyrapone N2 atom, which is very similar to the camphor carbonyl oxygen-Tyr-96 hydrogen bond in the camphor-bound structure (Figure 6A). Moreover, the mean temperature factor for the Tyr-96 segment is essentially the same in each structure.

The only significant movement of protein atoms in the metyrapone complex occurs in the distal helix region that forms part of the oxygen-binding pocket, residue 247-252 (Figure 4A). These residues must shift out away from the oxygen pocket, owing to the close approach of the inhibitor. The temperature factors in the camphor-bound and metyrapone-complexed structures are similar, indicating no large shifts in thermal motion. Overall, metyrapone causes the least shift in either atomic positions or thermal parameters of the four complexes examined.

1- and 4-Phenylimidazoles. With both of these inhibitors, an imidazole nitrogen atom coordinates directly with the iron atom. The phenyl ring protrudes into the camphor pocket and is situated near Phe-87 and Tyr-96, both of which contact the camphor molecule. As with metyrapone, both 1- and 4-phenylimidazoles force part of the distal helix to move away from the inhibitor (parts C and E of Figure 4).

1- and 4-phenylimidazole are oriented slightly differently in the active site and, as such, cause different degrees of repositioning of protein atoms. 4-Phenylimidazole causes the largest shifts, particularly in the region near Phe-87 and Tyr-96. The benzene ring of 4-phenylimidazole sits further from the native position of Phe-87 than the corresponding ring of 1-phenylimidazole, so Phe-87 must move further into the pocket in order to maintain good hydrophobic contacts with the inhibitor.

Localized changes in temperature factors also were observed. For both 1- and 4- phenylimidazoles, regions around Tyr-96 and Thr-185 undergo enhanced thermal motion in the inhibited complex. Thr-185 is centered in the loop connecting helices F and G, while Tyr-96 is situated at the C-terminal end of helix B. These are precisely the same regions that experience enhanced thermal motion in the camphor-free structure (Poulos et al., 1986). Indeed, the pattern of the temperature difference plots for 1- and 4-phenylimidazole (Figure 5) is essentially the same as we found in the camphor-free structure. Both the Tyr-96 and the Thr-185 regions contact the camphor molecule in the native structure but do not contact either 1- or 4-phenylimidazole. Thus, these segments exhibit higher thermal fluctuations due to the lack of inhibitor–protein interactions in the phenylimidazole complexes and the substrate-free enzyme. No increase in thermal motion was observed with metyrapone bound at the active site since this larger inhibitor does contact the same group of atoms (Tyr-96 and Thr-185) that contacts the camphor.

2-Phenylimidazole. A linear N–Fe bond on the order of 2.0 Å cannot form with 2-phenylimidazole as with the other inhibitors since the benzene ring would approach much too closely to the heme. As a result, an aqua ligand remains bound to the iron atom, while the inhibitor occupies the substrate pocket. Without direct coordination to the iron atom, one might anticipate two possible orientations of 2-phenylimidazole: one with the imidazole ring closest to the heme

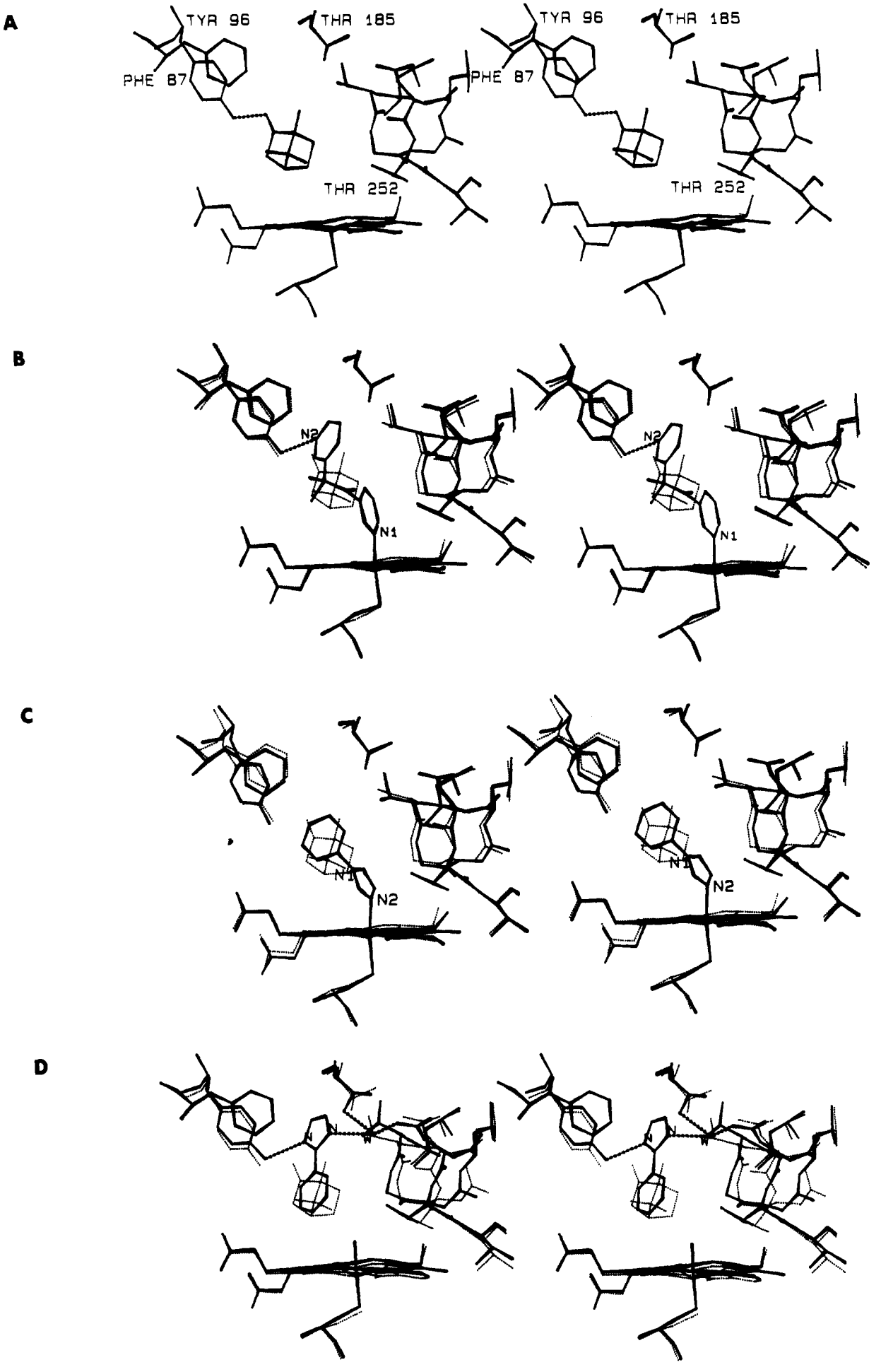
A
TYR 96
THR 185
PHE 87
THR 252
TYR 96
THR 185
PHE 87
THR 252
B
N2
N1
N2
N1
C
N1
N2
N1
N2
D

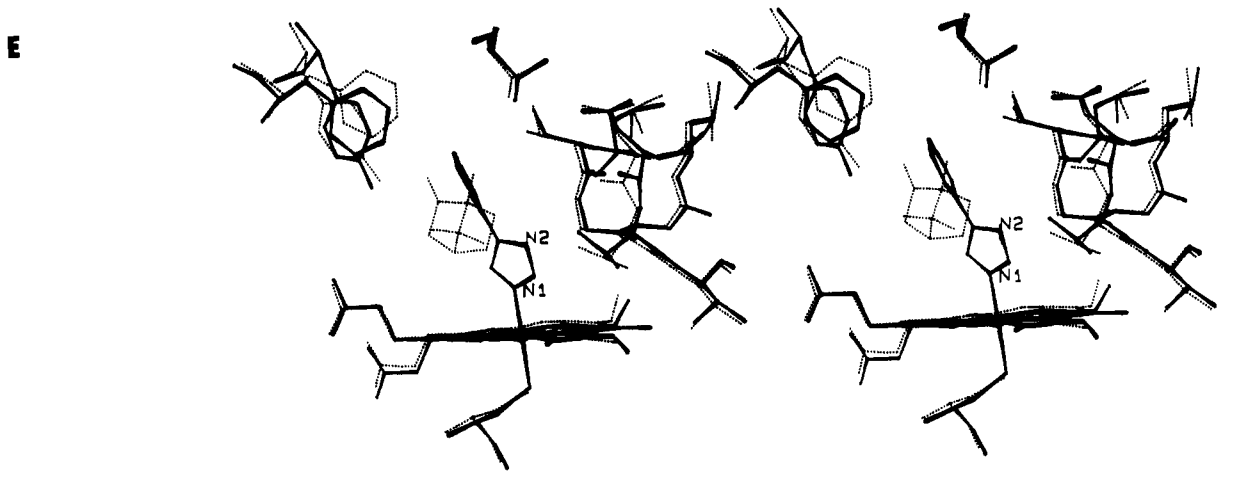

FIGURE 4: Final refined models superimposed on the native, camphor-bound structure. The dashed lines represent the camphor-bound structure and the solid lines the inhibited structure. (A) Native camphor-bound; (B) metyrapone; (C) 1-phenylimidazole; (D) 2-phenylimidazole; and (E) 4-phenylimidazole. Large changes in helix I are confined to residues 246–252. The largest shift in main-chain atoms was with 2-phenylimidazole, where the α carbon atom of Gly-249 moved approximately 2 Å closer to the inhibitor.

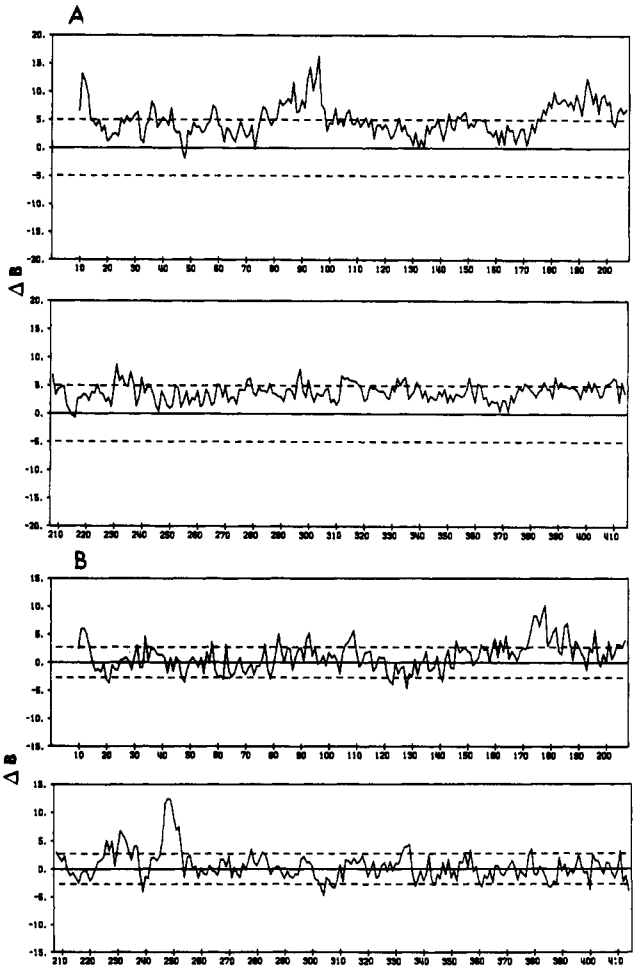

FIGURE 5: Plot of the difference in mean temperature factor between the camphor-bound and inhibited complexes as a function of residue number. The difference in mean temperature factor (ΔB) in square angstroms (inhibited – parent) is plotted along the Y axis and the residue number along the X axis. The dashed lines indicate the root mean square difference in mean temperature factors. (A) 1-Phenylimidazole – parent and (B) 2-phenylimidazole – parent. The metyrapone – parent difference showed no significant differences, while the pattern of changes with 4-phenylimidazole was the same as with 1-phenylimidazole.

and the second with the phenyl ring closest to the heme. Yet, as with metyrapone, there is a preferred orientation of the inhibitor. The benzene ring points down toward the heme, while the imidazole ring sits between Tyr-96 and Asp-251. This preferred orientation undoubtedly results from the hydrogen-bonding pattern shown in Figure 7. A new water molecule, labeled Wat in Figure 7, enters the active site to hydrogen bond with the inhibitor while Asp-251 moves in toward the active site to form a second hydrogen bond with this water molecule. The remaining imidazole nitrogen atom then hydrogen bonds with Tyr-96. The binding of the inhibitor and the addition of the new water molecule also are associated with movement of Thr-185 as indicated by $F_o - F_c$ difference maps. The movement of Thr-185 was best interpreted as a 180° rotation of the threonine side-chain about the C_α–C_β bond such that the side-chain hydroxyl group can interact with the new water molecule (Figures 4D and 7).

2-Phenylimidazole induces the largest change in the distal helix of the inhibitors examined. Shifts up to 2.0 Å were found in the movement of main-chain atoms in the region of the helix I spanning Gly-247 to Asn-255, demonstrating a large degree of flexibility in the distal helix. Moreover, the direction of helix I movement is opposite to that found with the other inhibitors. That is, helix I moves *in* toward the inhibitor rather than *away* as with the other inhibited complexes. Accompanying this conformational change was a large increase in temperature factors in the same region (Figure 6C). As with metyrapone, however, the Tyr-96 region does not experience a large change in thermal motion, presumably because Tyr-96 hydrogen bonds with both inhibitors. The Thr-185 region, however, does experience enhanced thermal motion but not to the extent that was found with 1- and 4-phenylimidazoles.

Discussion

Thermal Motion. From a comparison of shifts in atomic coordinates and changes in mean temperature factors, the metyrapone complex was found to most closely resemble the camphor-bound structure. No large shifts in atomic positions or temperature factors were observed with the exception of helix I. On the other hand, 1- and 4-phenylimidazole more closely resemble the camphor-free structure in that the pattern of increased dynamical fluctuation (Figure 5) in the phenylimidazole complexes was exactly the same as we observed in the camphor-free structure. These differences and similarities can best be explained by considering perturbations near Phe-87/Tyr-96 and Thr-185, both of which contact the camphor molecule in the enzyme–substrate complex. Metyrapone makes the same series of contacts that camphor does, most notably a hydrogen bond with Tyr-96 and a hydrophobic contact with the side-chain methyl group of Thr-185. Neither

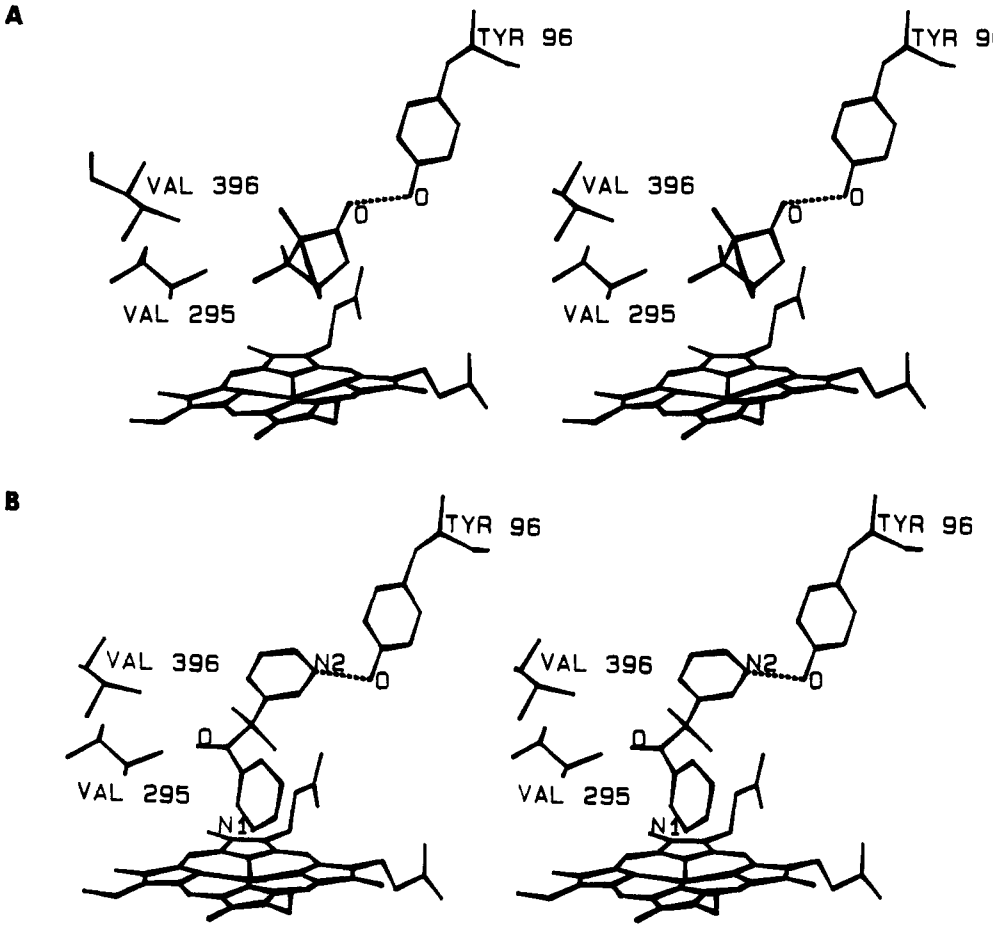

FIGURE 6: Comparison of the metyrapone-inhibited and camphor-bound structures highlighting the interactions with Tyr-96, Val-295, and Val-396: (A) parent and (B) metyrapone.

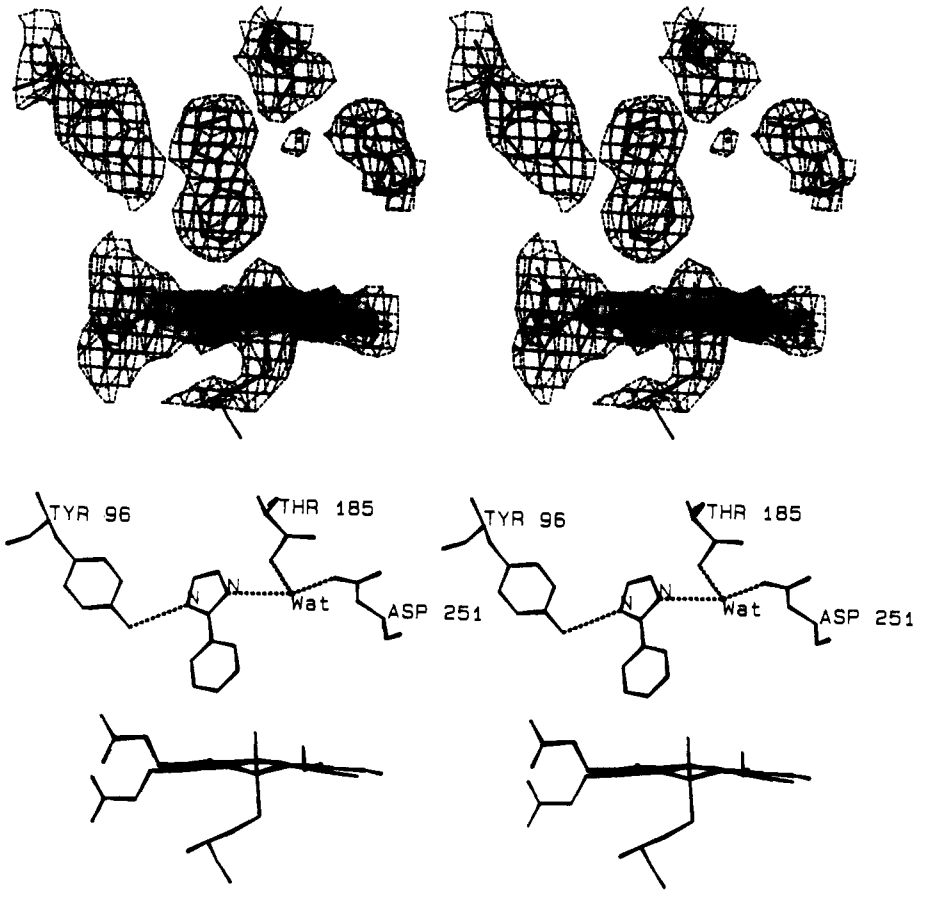

FIGURE 7: More detailed view of the hydrogen-bonding interactions in the 2-phenylimidazole-inhibited complex.

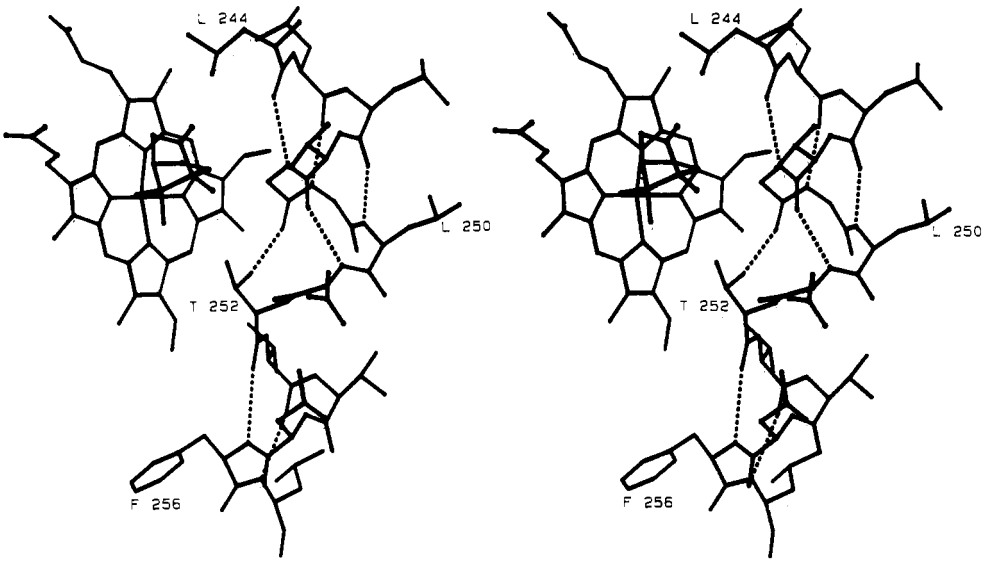

FIGURE 8: Region of the distal helix or helix I in the immediate vicinity of the oxygen-binding pocket. Dashed lines indicate hydrogen bonding. Notice the distortion in the normal helical hydrogen-bonding pattern centered on Thr-252. This produces a local opening in the helix that forms part of the oxygen-binding pocket. This local disruption of the helix and the Thr-252 side-chain OH to Gly-248 peptide carbonyl oxygen hydrogen bond are maintained in all the inhibited complexes despite the relatively large shift in helix I.

1- nor 4-phenylimidazole, however, contacts Tyr-96 or Thr-185, leading to large dynamical fluctuations in these regions exactly as we observed in the camphor-free structure. That similar temperature factor increases relative to the camphor-bound enzyme have now been observed in three different forms of P-450$_{cam}$ further underscores the importance that dynamical fluctuations play in substrate binding. Moreover, these observations provide an explanation to a puzzling problem regarding how the camphor gains access to its binding pocket. The P-450$_{cam}$ active site does not form a cleft at the molecular surface as in many other enzymes but, instead, the camphor is almost completely buried except for a small opening directly above the substrate-binding pocket. This opening is near the loop connecting helices F and G and the turn connecting the two antiparallel β strands of β5 (Figure 2). Even though this opening is too small to accommodate a camphor molecule, those regions undergoing enhanced fluctuations in the 1-phenylimidazole, 4-phenylimidazole, and camphor-free structures are just those regions that define the substrate entry channel. It therefore appears that dynamical fluctuations are important in allowing entry of a substrate molecule.

2-Phenylimidazole and the Flexible Distal Helix. The binding mode of 2-phenylimidazole is considerably different from that of the other inhibitors since steric constraints prevent formation of the N–Fe bond. Nevertheless, it is similar to the metyrapone-complexed and camphor-bound enzyme in that Tyr-96 hydrogen bonds with the complexed molecule, in this case an imidazole nitrogen atom. The resulting decreased flexibility of Tyr-96 relative to the non-hydrogen-bonded situations is reflected in a similar mean temperature factor for Tyr-96 in the 2-phenylimidazole, metyrapone, and camphor-bound structures.

All the inhibitors force helix I to move away from the O_2 binding site with the single exception of 2-phenylimidazole. With this inhibitor the central region of helix I moves in toward the inhibitor, and the movements are much larger, up to 2 Å, than were observed with the other inhibitors. Moreover, there also is sufficient room for a water molecule to hydrogen bond with both Asp-251 and the inhibitor's imidazole group (Figure 7). If helix I had not moved, a considerable gap would exist between helix I and the inhibitor. Therefore, the readjustment in helix I is required to optimize the Asp-251–water–inhibitor hydrogen bonds as well as to optimize nonbonded contacts between the inhibitor and helix I. If this explanation is correct, it raises some interesting energetic considerations. The estimated binding constant for 2-phenylimidazole (Lipscomb, 1980) indicates a ΔG of about −7 cal/mol, which is very near to that of camphor itself (Gunsalus et al., 1974; Griffin & Peterson, 1972). As with camphor, the primary driving force very likely is the entropically favored release of solvent molecules that occupy the active site in the absence of inhibitors or substrate (Poulos et al., 1986) in addition to the entropically favored transfer of the benzene moiety from the solvent to the protein interior. Replacement of bulk solvent–imidazole interactions by protein–imidazole interactions and nonspecific hydrophobic contacts probably contribute at most a few kilocalories to the free energy of binding. The same can be said for the carbonyl oxygen atom of camphor (Poulos et al., 1986). This suggests that the activation energy barrier for movement of helix I is quite low.

A closer examination of helix I in the vicinity of conformationally flexible region reveals an interesting local distortion in the helical hydrogen-bonding pattern (Figure 8). In a normal α helix, the peptide NH of Thr-252 would accept a hydrogen bond from the carbonyl oxygen atom of Gly-248. Instead, the Gly-248 peptide oxygen atom points away from the helical axis to accept a hydrogen bond from the side-chain OH group of Thr-252. This helps to stabilize a local widening and kinking of the helix, which we believe is required to form the O_2-binding pocket (Poulos et al., 1987). Moreover, sequence alignments demonstrate a high degree of homology near Thr-252, indicating a similar O_2 pocket in eukaryotic P-450s (Poulos et al., 1985). Therefore, those residues of helix I that move the most in response to inhibitor binding, and especially with 2-phenylimidazole binding, are the same residues involved in a functionally important and probably highly conserved part of the active site involved in O_2 binding. The hydrogen-bonding pattern designed to stabilize the local helical distortion is maintained even after the inhibitor-induced conformational change. At least part of the reason for the helical flexibility is the Gly–Gly sequence (residues 248–249), which is either Gly–Gly or Ala–Gly in all P-450s for which sequence data are available (Poulos et al., 1985). The local

helical distortion and hydrogen bonding involving Thr-252 and Gly-248 are maintained in all the inhibited structures despite the relatively large shifts in helix I. These results illustrate that a conserved and functionally important region of P-450 can tolerate a significant perturbation yet maintain critical intramolecular hydrogen bonds.

Structural Basis for Spectroscopic and Binding Results. With the availability of spectroscopic data, equilibrium binding data, and crystal structures, it is tempting to try and provide a structural basis for observed differences in binding constants and spectroscopic properties. Dawson et al. (1982) and Lipscomb (1980) have studied these inhibitors using EPR, visible absorption, and magnetic circular dichroism spectroscopy. Each forms low-spin complexes as expected in forming the N–Fe bond. Dawson et al. noted, however, that 2-phenylimidazole, indole, and benzimidazole were "unusual" since the spectroscopic properties of these complexes so closely matched those of low-spin, substrate, and inhibitor-free P-450$_{cam}$. We can now offer a structural basis for these results. Owing to steric constratints, 2-phenylimidazole cannot form an N–Fe bond but instead binds in the substrate pocket adjacent to the oxygen-binding site with water or hydroxide linked to the iron atom. Thus, the coordination environment of the iron atom is exactly the same as in the low-spin native enzyme: hexacoordinate with an aqua ligand trans to the cysteine ligand. Not surprisingly, the spectroscopic properties are very similar. It would appear that benzimidazole and indole exhibit the same binding patterns as 2-phenylimidazole.

The simplest case for correlating binding constants and structure is with 1- and 4-phenylimidazole since the dissociation constants are very different, 0.0001 mM for 1-phenylimidazole and 0.04 mM for 4-phenylimidazole (Lipscomb, 1980). One of the most important and obvious differences in the two inhibitors is that once bound to the enzyme 4-phenylimidazole has one free imidazole nitrogen atom, while the 1-isomer has none. In considering the energetics of binding, one must take into account this difference and its relationship to the thermodynamics of desolvating the inhibitor imidazole group as it transfers from solution to the protein's interior. While the free nitrogen atoms of both 2-phenylimidazole and metyrapone hydrogen bond with groups at the active site, the free N2 of 4-phenylimidazole has no similar sets of interactions (Figure 4E) and remains essentially "unsolvated". Therefore, transfer of the 4-phenylimidazole imidazole ring from solution to the active site is thermodynamically less favorable than the corresponding transfer in 1-phenylimidazole that has no free, unliganded nitrogen atoms. Notice, too, that the orientation of the two inhibitors in the active site is very different (Figure 4C,E). In the 1-isomer, the plane of the imidazole ring is roughly parallel to the helix I axis, enabling hydrophobic contacts between the inhibitor imidazole carbon atoms and α carbon atoms of helix I. With the 4-isomer, the imidazole ring is nearly perpendicular to the axis of helix I. As a result, the lone pair of N2 in the 4-isomer points toward the local widening and kinking of helix I near Thr-252 that we have postulated is the O_2-binding pocket. In this conformation, N2 is as close as possible to a potential hydrogen-bonding group, 4.2 Å from the side-chain hydroxyl group of Thr-252, and as close as possible to the nearest solvent molecule, about 7 Å, though too far for strong interactions. Apparently, the imidazole ring is oriented in an attempt to "solvate" the N2 lone pair yet maintain the N1–Fe bond. This requires that the benzene ring of the 4-isomer be situated further from Phe-87 than in the 1-isomer, thus requiring a relatively large movement of Phe-87 in order to maintain contact with the inhibitor benzene ring. In the 1-isomer, the imidazole ring is oriented more favorably, allowing the inhibitor benzene ring to contact Phe-87 without a repositioning of Phe-87. Taken together, these differences offer a qualitative explanation for the 400-fold difference in binding constants for 1- and 4-phenylimidazole.

ACKNOWLEDGMENTS

We thank Dr. I. C. Gunsalus for the purified P-450$_{cam}$ and Dr. B. C. Finzel for assistance with crystallographic refinement.

REFERENCES

Black, S. D., & Coon, J. J. (1986) in *Cytochrome P450: Structure, Mechanism, and Biochemistry* (Ortiz de Montellano, P., Ed.) pp 161–216, Plenum, New York.

Dawson, J. H., Anderson, L. A., & Masanori, S. (1982) *J. Biol. Chem. 257*, 3606–3617.

Debrunner, P. G., Gunsalus, I. C., Sligar, S. G., & Wagner, G. C. (1978) in *Metals in Biological Systems* (Siegel, H., Ed.) Vol. 7, pp 241–275, Marcel Dekker, New York.

Dominguez, O. V., & Samuels, L. T. (1963) *Endocrinology (Baltimore) 73*, 304–309.

Finzel, B. C., & Salemme, F. R. (1985) *Nature (London) 315*, 686–688.

Frauenfelder, H., Petsko, G. A., & Tsernoglou, D. (1979) *Nature (London) 280*, 558–563.

Gelb, M. H., Heimbrook, D. C., Malkonen, P., & Sligar, S. (1982) *Biochemistry 21*, 370–377.

Griffin, B. W., & Peterson, J. A. (1972) *Biochemistry 11*, 4740–4746.

Gunsalus, I. C., & Sligar, S. G. (1978) *Adv. Enzymol. Relat. Areas Mol. Biol. 47*, 1–44.

Gunsalus, I. C., Meeks, J. R., Lipscomb, J. D., Debrunner, P. G., & Munck, E. (1974) in *Molecular Mechanisms of Oxygen Activation* (Hayaishi, O., Ed.) Chapter 14, Academic, New York.

Hayaishi, O. (1974) *Molecular Mechanisms of Oxygen Activation*, Academic, New York.

Hendrickson, W. A., & Konnert, J. H. (1980) in *Computing in Crystallography* (Diamond, R., Ramaseshan, S., & Venkatesan, K., Eds.) pp 1301–1323, Indian Institute of Science, Bangalore.

Honzatko, R. B. (1986) *Acta Crystallogr., Sect. A: Found. Crystallogr. A42*, 172–178.

Karplus, M., & McCammon, J. A. (1983) *Annu. Rev. Biochem. 53*, 263–300.

Lipscomb, J. D. (1980) *Biochemistry 19*, 3590–3599.

Poulos, T. L., Perez, M., & Wagner, G. C. (1982) *J. Biol. Chem. 257*, 10427–10429.

Poulos, T. L., Finzel, B. C., Gunsalus, I. C., Wagner, G. C., & Kraut, J. (1985) *J. Biol. Chem. 260*, 16122–16130.

Poulos, T. L., Finzel, B. C., & Howard, A. J. (1986) *Biochemistry 25*, 5314–5322.

Poulos, T. L., Finzel, B. C., & Howard, A. J. (1987) *J. Mol. Biol. 195*, 687–700.

Testa, B., & Jenner, P. (1981) *Drug Metab. Rev. 12*, 1–117.

Van Gunsteren, W. F., & Karplus, M. (1981) *Nature (London) 293*, 677–678.

Wagner, G. C., & Gunsalus, I. C. (1982) in *The Biological Chemistry of Iron* (Dunford, H. B., Dolphin, D., Raymond, K., & Sieker, L., Eds.) pp 405–412, Riedel, Boston.